

**Photocatalysis**

# Electron-Poor Acridones and Acridiniums as Super Photooxidants in Molecular Photoelectrochemistry by Unusual Mechanisms

Jonas Žurauskas<sup>+</sup>, Soňa Boháčová<sup>+</sup>, Shangze Wu, Valeria Butera, Simon Schmid, Michał Domański, Tomáš Slanina, and Joshua P. Barham\*

**Abstract:** Electron-deficient acridones and in situ generated acridinium salts are reported as potent, closed-shell photooxidants that undergo surprising mechanisms. When bridging acyclic triarylamine catalysts with a carbonyl group (acridones), this completely diverts their behavior away from open-shell, radical cationic, ‘beyond diffusion’ photocatalysis to closed-shell, neutral, diffusion-controlled photocatalysis. Brønsted acid activation of acridones dramatically increases excited state oxidation power (by +0.8 V). Upon reduction of protonated acridones, they transform to electron-deficient acridinium salts as even more potent photooxidants ( $E_{1/2}^* = +2.56\text{--}3.05\text{ V vs SCE}$ ). These oxidize even electron-deficient arenes where conventional acridinium salt photooxidants have thus far been limited to electron-rich arenes. Surprisingly, upon photoexcitation these electron-deficient acridinium salts appear to undergo *two electron reductive quenching* to form acridinide anions, spectroscopically-detected as their protonated forms. This new behaviour is partly enabled by a catalyst preassembly with the arene, and contrasts to conventional SET reductive quenching of acridinium salts. Critically, this study illustrates how redox active chromophoric molecules initially considered photocatalysts can transform during the reaction to catalytically active species with completely different redox and spectroscopic properties.

## Introduction

In recent years, chemists have identified the need for a shift in chemical redox feedstocks – away from those that are heavily-functionalized, atom uneconomical and require several preparation steps – toward those directly available from petrochemicals, chemical waste, or biomass. However, as typical thermodynamic sinks such molecules are challenging to engage in redox processes. Thus, engaging ‘unactivated’ organic molecules ( $E^0 \geq \pm 2.0\text{ V vs SCE}$ ) in redox reactions under mild reaction conditions has become a high priority synthetic target transformation. Photoredox catalysis (PRC) offered promise in leveraging visible light energy for reasonably powerful single electron transfer (SET) redox processes (substrates with  $E^0 \leq \pm 2.0\text{ V vs SCE}$ ),<sup>[1]</sup> but it is limited by the single photon energy. An effective and general strategy to exceed this limit is the photoexcitation of radical ions that are generated electrochemically (i.e., electro-activated Photoredox Catalysis, ‘e-PRC’)<sup>[2,3]</sup> or in consecutive Photoinduced Electron Transfer (‘conPET’).<sup>[4]</sup> While much progress has been achieved using single catalyst systems in PRC<sup>[5]</sup> and conPET<sup>[6]</sup> for deeply reductive transformations, fewer developments have been achieved in the deeply oxidative direction<sup>[7]</sup> and far fewer examples in the case of conPET.<sup>[8]</sup> On the other hand, e-PRC has proven effective for oxidative functionalizations of unactivated molecules with exquisite selectivity under mild conditions.<sup>[9]</sup>

Triarylamine derivatives are a privileged precatalyst scaffold for e-PRC and conPET reactions (Figure 1),<sup>[8,9b]</sup> due to remarkable stability of their radical cationic forms and their rich history of photophysical characterization.<sup>[10]</sup> First reported by Moutet and Reverdy, the electrogenerated *N*-phenyl phenothiazine radical cation (**PTZ**<sup>•+</sup>) was photoexcited to SET oxidize unactivated styrenes,<sup>[11]</sup> albeit in poor catalytic turnover. Wagenknecht and co-workers later leveraged PET-generated, photoexcited **PTZ**<sup>•+</sup> to oxidize styrenes in a pentafluorosulfonylation reaction.<sup>[8b]</sup> In 2021, Barham and co-workers disclosed electrogenerated acyclic tri(*para*-substituted biaryl)aminiums (**TPA**<sup>•+</sup>s) as tunable ‘super’ oxidants for arenes in an azolation reaction.<sup>[9b]</sup> The *para*-cyanophenyl derivative (**TCBPA**) engaged PhCl and even PhF in SET oxidations, arising azolated products in useful yields (65 %, 45 %), however was a high M.W. catalyst. Later that year, Wickens and co-workers reported arene azolations using **PTZ** in a conPET fashion with O<sub>2</sub> as the electron sink.<sup>[8c]</sup> While **PTZ** was a more compact (low M.W.) catalyst and was effective for moderately challenging

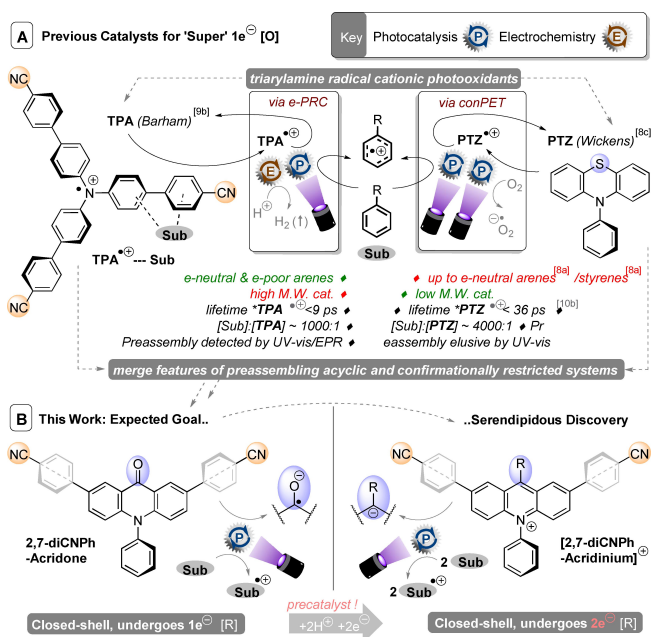
[\*] J. Žurauskas,<sup>+</sup> Dr. S. Wu, S. Schmid, M. Domański, Dr. J. P. Barham  
 Institute of Organic Chemistry, University of Regensburg  
 Universitätsstr. 31, 93053 Regensburg (Germany)  
 E-mail: Joshua-Philip.Barham@chemie.uni-regensburg.de

Dr. S. Boháčová,<sup>+</sup> Dr. T. Slanina  
 Institute of Organic Chemistry and Biochemistry, Academy of  
 Sciences of the Czech Republic  
 Flemingovo nám. 2, 16000 Prague 6 (Czech Republic)

Dr. V. Butera  
 Central European Institute of Technology, CEITEC, 61200 Brno  
 (Czech Republic); Department of Science and Biological Chemical  
 and Pharmaceutical Technologies, University of Palermo, 90128,  
 Palermo (Italy)

[†] These authors contributed equally to this work.

© 2023 The Authors. Angewandte Chemie International Edition published by Wiley-VCH GmbH. This is an open access article under the terms of the Creative Commons Attribution License, which permits use, distribution and reproduction in any medium, provided the original work is properly cited.



**Figure 1.** A: Previous triarylamine radical cation open-shell super photooxidants. B: Acridone and acridinium salt closed-shell super photooxidants.

arenes (benzene or methylated arenes), oxidation of PhCl was low yielding (only 22 % of azolated product).

A general challenge is that ultrashort excited state lifetimes of photoexcited radical ions ( $\leq 9$  ps for \*TCBPA<sup>•+</sup>,<sup>[9b]</sup>  $\leq 36$  ps for \*PTZ<sup>•+</sup><sup>[10b]</sup>) prohibit diffusion-controlled bimolecular chemistry. To outcompete excited state deactivation, productive photochemistry needs the target substrate in a close proximity to the radical cation, which either requires i) an organized preassembly or ii) a vast enough excess of substrate such that statistically there is likely to be an arene close enough.<sup>[12]</sup> Our group found steady-state spectroscopic, reactivity and computational evidence of radical ion-substrate preassemblies in e-PRC studies<sup>[9b,13]</sup> such as that on TPA<sup>•+</sup>. However, evidence of preassemblies eluded most conPET studies proposed to proceed by ultrashort-lived excited radical ions,<sup>[6]</sup> such as for the case for PET-generated PTZ<sup>•+</sup>.<sup>[8c]</sup> While a lack of changes in steady-state spectroscopy does not rule out a preassembly,<sup>[13]</sup> its existence can and has been confirmed by detailed transient absorption spectroscopy investigations for both radical cation and anion systems.<sup>[14]</sup>

Although photoexcited radical ions were confirmed as the catalytically-active species in several cases (spectroscopically and through their isolation as authentic species),<sup>[12,14,15]</sup> such reaction mechanisms previously attracted controversy.<sup>[16]</sup> Alternative proposals have been made such as i) release of solvated electrons<sup>[17,18]</sup> and ii) decomposition of photoactive radical ions to longer lived closed-shell photocatalysts.<sup>[16b]</sup> These specific cases highlight – in a broader sense – mechanistic complexities in the field of PRC that are not accounted for by initially, naïvely drawn catalytic cycles.<sup>[19]</sup> Moreover, subtle modifications to the catalyst structure or its aggregation state<sup>[13,20,21]</sup> can com-

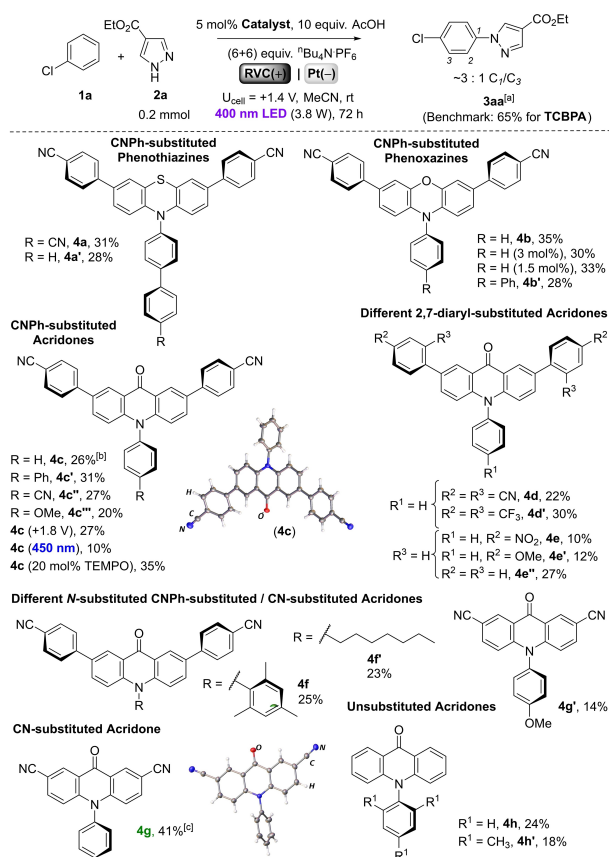
pletely divert the reaction mechanism. Moreover, the ‘catalyst’ the chemist adds to the reaction *may not necessarily be the active catalyst*; decomposition to another catalytically active species is becoming a common theme.<sup>[22]</sup> However, such possibilities have not been rigorously interrogated in oxidative photocatalyst systems.

Concerning the triarylamine ‘super’-oxidation precatalysts, simplifying the radical cationic systems and circumventing the need for preassembly would be a ‘closed-shell’ potent neutral photooxidant that could somehow achieve ‘super’ oxidations within the single photon energy limit. Herein, we report i) novel acridone catalysts as potent neutral SET photooxidants ( $E^0$  up to a +2.49 V vs SCE) and ii) transformation of the acridone under the reaction conditions into a novel acridinium salt with a record-breaking<sup>[14,7i]</sup> redox potential for oxidation ( $E^0$  up to +2.56–3.05 V vs SCE) that, surprisingly, appears to function by *two electron reduction* of its excited state. To date, photoexcited acridinium salts were only reported as one electron oxidants.

## Results and Discussion

**Catalyst Structure-Activity Relationship:** We were curious as to the aforementioned mechanistic discrepancies between TPA<sup>•+</sup> and PTZ<sup>•+</sup> (detection of substrate assembly or lack thereof) and postulated this may arise from the conformationally flexible vs restricted nature of the scaffolding around the N radical cation. As our starting point, we set about synthesizing a library of hybrid catalysts combining the semi-cyclized core of PTZ<sup>•+</sup> with the preassembling 4-substituted biphenyl (4-cyanophenyl) units of TPA<sup>•+</sup>. Phenothiazines, phenoxazines and acridones were chosen as parent core compounds for the catalyst library, where *N*-substituents were installed by Buchwald–Hartwig couplings or alkylation reactions. The 2,7-dibromides were prepared by bromination with Br<sub>2</sub>, and then coupled via Suzuki reactions with arylboronic acids. This afforded 2,7-dicyanophenylated phenothiazines (**4a** and **4a'**, Scheme 1) in high (83–88 %) yields and 2,7-dicyanophenylated phenoxazines (**4b** and **4b'**) also in high (84–85 %) yields. The more electron-deficient 2,7-dibrominated acridones were harder to arylate, affording products (**4c-4e'**) in good to high (59–77 %) yields.

The 2,7-diarylated semi-cyclic triarylamine catalysts were then screened against acyclic TCBPA (yielding 65 % of **3aa**)<sup>[9b]</sup> in the e-PRC oxidative C–H azolation of chlorobenzene (Scheme 1). Upon subjecting to applied potential ( $U_{\text{cell}} + 1.4$  V), phenothiazines (**4a**) as well as phenoxazines (**4b**) underwent rapid color change from yellow to deep green solutions,<sup>[23]</sup> which, together with their matching redox potentials ( $E_{1/2}(\mathbf{4a}^{\bullet+}/\mathbf{4a}) + 0.78$  V;  $E_{1/2}(\mathbf{4b}^{\bullet+}/\mathbf{4b}) + 0.79$  V vs SCE) and spectroelectrochemistry (see Supporting Information (SI) file) confirmed radical cation formation. However, their catalytic reactions afforded only modest yields of **3aa** (ca. 30 %), and the *N*-(*p*)-biphenyl substituted compounds performed similarly, if slightly worse. Concerned that the deep green solutions led to too much screening of 400 nm



**Scheme 1.** Screening of semi-cyclic triarylamine catalysts in the C–H azolation of PhCl. General reaction scheme (top), catalyst structures and respective yields (bottom). <sup>[a]</sup>Yield determined by <sup>1</sup>H NMR using CH<sub>2</sub>Br<sub>2</sub> (200 mol%) as an internal standard. <sup>[b]</sup>Average of 3 replicates. <sup>[c]</sup>Average of 2 replicates. For XRD crystal structures of **4c** and **4g**: H atoms (white), C atoms (grey), N atoms (blue) and O atoms (red).

light, we investigated decreased catalyst loadings of **4b** but this made no difference.

We were surprised to see that despite its less accessible redox potential ( $E_{1/2}(\mathbf{4c}^{\bullet+}/\mathbf{4c}) = +1.49\text{ V}$  vs SCE) due to the electron-withdrawing bridging carbonyl group, 2,7-dicyanophenylated acridone **4c** still performed comparably (26% **3aa**) to its phenothiazine and phenoxazine cousins. Acridone derivatives have scarcely been employed in synthetic photochemistry,<sup>[24]</sup> and this type of electron-deficient acridone has not been examined previously. Noticing that the redox potential for oxidation of **4c** likely exceeds the applied cell potential, a higher potential ( $U_{\text{cell}}$ ) of +1.8 V was applied but the yield of **3aa** was unchanged. Notably, no initial color change occurred in the reactions of **4c**, in direct contrast to **4a**, **4b** and TCBPA, suggesting a different mechanism operated. When 450 nm was used, the yield of **3aa** was low (10%) but not negligible even though **4c** barely absorbs at 450 nm compared to **4a** and **4b** (see SI file). We note that no reaction at all was observed for TCBPA at 450 nm in our previous study.<sup>[9a]</sup> The presence of TEMPO (20 mol%) did not inhibit the reaction.

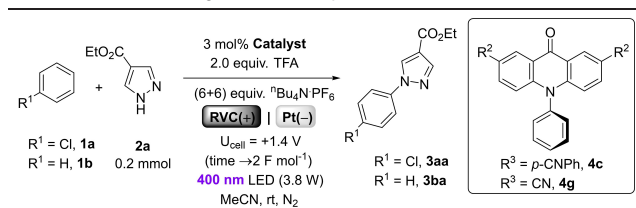
The catalytic system was relatively insensitive to *para*-modifications at N–Ar (**4c** vs. **4c'**, **4c''**); only an electron-

rich substituent (**4c'''**) decreased the yield of **3aa**. The catalytic system was somewhat more sensitive to modifications at the 2,7-aryl groups. While two trifluoromethyl substituents performed similarly to a single cyano substituent or no substituents (**4d'** vs. **4c/4e''**), too strongly electron-withdrawing substituents (**4d** and **4e**) or too strongly electron-donating (**4e'**) substituents notably decreased performance. Even *N*-substituents known to promote or obviate charge transfer behavior – *N*-methyl (**4f**) and *N*-heptyl (**4f'**) – gave similar performances to **4c**. These results suggested the acridone core was the most important aspect for catalytic activity. At this juncture, we investigated direct cyanation at the 2,7-positions of the acridone core. Therefore, 2,7-dicyanoacridones were prepared via a Rosemund-von Braun cyanations of their 2,7-dibrominated acridone precursors in high (81–88%) yields. Acridone **4g** outperformed all other derivatives (41% **3aa**) including its *N*-anisole congener **4g'**, its parent *N*-phenyl acridone **4h** or the *N*-mesityl derivative **4h'**. Although **4g** still did not outperform TCBPA (65% **3aa**) under comparable conditions, we opted to proceed it to reaction optimization (Table 1) and substrate scope due to its attractions as a more compact (lower M.W.) catalyst that likely proceeded via a *different mechanism* than acyclic TPAs.

**Arene Azolation Optimization:** Results of **4c** and **4g** are shown in Table 1 (entries 1, 3). **4c** gave no conversion in the absence of electrochemical conditions (electrodes/potential/electrolyte and protic source, entry 2). Pleasingly, decreasing the catalyst loading to 3 mol% while employing a stronger protic source TFA (2 equiv.) increased the yield of **3aa** to 51% (entry 4). Benzene gave a lower yield of **3ba** under these conditions (entry 5), but we decided to progress optimization with it due to the single regioisomer product being easier to analyze. We hypothesized that the cathodic half-reaction (HER) might be limiting due to the lower surface area of the coiled Pt wire cathode vs the RVC anode. Gratifyingly, use of pre-platinized RVC – prepared from K<sub>2</sub>[PtCl<sub>4</sub>] as the precursor (see SI file for details and SEM images) – as cathode increased the yield to 80% (entry 6). A control experiment spiking K<sub>2</sub>[PtCl<sub>4</sub>] did not increase the yield of the Pt wire reaction (entry 7 vs 5), and a control reaction without electrochemical conditions gave very poor conversion (entry 8). As with **4c** (Scheme 1), the addition of TEMPO did not inhibit the reaction catalyzed by **4g** (entry 9 vs 6). Nicewicz and co-workers reported that TEMPO dramatically enhanced conversion in arene azolations<sup>[7b]</sup> by acridinium PRC, as a HAT shuttle, but for these acridones catalysts (**4c**, **4g**) the mechanism differs.

Cobalt co-catalysts have been reported to promote arene azolation reactions,<sup>[7c]</sup> however addition of [Co<sup>II</sup>] was unproductive (entry 10). Further doubling the cathodic surface area (2× Pt-RVC) did not improve efficiency and other electrolytes gave poorer results (see SI). Constant current (CC) conditions (0.5 mA) could be employed (entries 11–13). While running to 3 Fmol<sup>-1</sup> led to decomposition and 1 Fmol<sup>-1</sup> insufficient conversion of **2a**, running to 2 Fmol<sup>-1</sup> gave **3ba** in 70% yield after only 25 h. However, we observed full deplatinization of the Pt-RVC cathode under CC conditions by SEM and so deemed constant potential



**Table 1:** Initial Investigations and Optimization of Conditions.


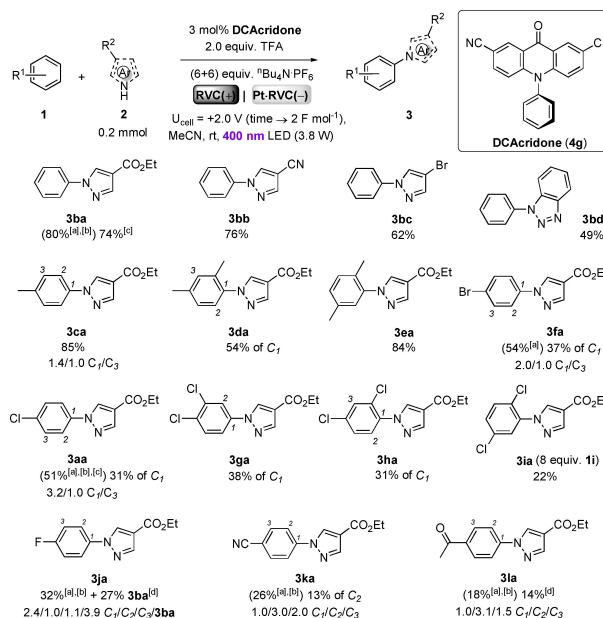
Entry	1/4	Deviations from Standard Conditions	Yield 3 <sup>[a]</sup>
1	1a/4c	5 mol% 4c, 10 equiv. AcOH, no TFA	26% 3aa (72 h) <sup>[b]</sup>
2	1a/4c	5 mol% 4c, no U <sub>cell</sub> , no electrolyte/electrodes, no AcOH	0% 3aa (72 h) <sup>[b]</sup>
3	1a/4g	5 mol% 4g, 10 equiv. AcOH, no TFA	41% 3aa (72 h) <sup>[b]</sup>
4	1a/4g	-	51% 3aa (70 h) <sup>[b]</sup>
5	1b/4g	-	35% 3ba (60 h) <sup>[b]</sup>
6	1b/4g	Pt-RVC(-)	80% 3ba (60 h)
7	1b/4g	K <sub>2</sub> [PtCl <sub>4</sub> ] (20 mol%)	35% 3ba (44 h) <sup>[b]</sup>
8	1b/4g	no U <sub>cell</sub> , no electrolyte/electrodes, no TFA	12% 3ba (70 h)
9	1b/4g	Pt-RVC(-), TEMPO (20 mol%)	74% 3ba (60 h)
10	1b/4g	Pt-RVC(-), Co(OAc) <sub>2</sub> (20 mol%)	45% 3ba (60 h)
11	1b/4g	Pt-RVC(-), 0.5 mA (→3 F mol <sup>-1</sup> )	41% 3ba (38 h) <sup>[d]</sup>
12	1b/4g	Pt-RVC(-), 0.5 mA (→1 F mol <sup>-1</sup> )	47% 3ba (14 h) <sup>[d]</sup>
13	1b/4g	Pt-RVC(-), 0.5 mA (→2 F mol <sup>-1</sup> )	70% 3ba (25 h) <sup>[d]</sup>
14	1b/4g	Pt-RVC(-), +2.0 V (→1 F mol <sup>-1</sup> ), 6 mol% 4g	47% 3ba (25 h)
15	1b/4g	Pt-RVC(-), +2.0 V (→1 F mol <sup>-1</sup> ), 1,2-DCE as solvent	< 5% 3ba (25 h)
16	1b/4g	Pt-RVC(-), +2.0 V (→1 F mol <sup>-1</sup> ), 365 nm LED <sup>[d]</sup>	27% 3ba (25 h)
17	1b/4g	Pt-RVC(-), +2.0 V (→1 F mol <sup>-1</sup> ), 10 equiv. MeOH, no TFA	35% 3ba (55 h)
18	1b/4g	Pt-RVC(-), +2.0 V (→1 F mol <sup>-1</sup> ), 0.5 mL 1b	31% 3ba (25 h)
19	1b/4g	Pt-RVC(+), RVC(-), +2.0 V (→1 F mol <sup>-1</sup> )	9% 3ba (25 h)

Unless otherwise stated, reactions were run to 2 or 1 F mol<sup>-1</sup> rather than under constant time to ensure comparability. 1.0 mL of arene was employed. [a] Yield of 3aa or 3ba determined by <sup>1</sup>H NMR using 1,3,5-trimethoxybenzene as an internal standard. [b] F mol<sup>-1</sup> not measured, stopped at the specified time. [c] Constant current was used. [d] See Supporting Information for details on different wavelengths.

conditions to be more robust for substrate scope. The strong influence of cathodic surface area suggested that catalytic turnover might be limited by the electrochemical step rather than the photochemical step, a behavior more consistent with ‘recycling’ e-PRC<sup>[2b]</sup> (than ‘radical ion’ e-PRC); where a spent closed-shell photocatalyst is electrochemically regenerated. Control reactions without 4g or without light gave no reaction (see SI). Other factors investigated included different catalyst loadings, solvents, arene loadings, LED

wavelengths and protic sources. We also reversed the electrode materials. However, these were not productive (entries 14–19) and we proceeded the conditions of entry 6.

**Arene Azolation Scope:** Benzene (1a) was arylated with different azole derivatives (Scheme 2) including cyano- and bromo-substituted pyrazoles as well as benzotriazole, affording products 3bb–3bd in good to high (49–78%) isolated yields. More electron-rich alkyl-substituted arenes toluene and xylenes gave good to high (56–85%) isolated yields (3ca–3ea). Previous radical cation photocatalytic reports always favored *m*-xylene over *p*-xylene presumably due to steric factors involved in the necessary preassembly,<sup>[9a,b]</sup> while here *p*-xylene was favored. Moreover, bromobenzene was azolated in a higher efficiency (54%) than any previous reports (≈30–35%).<sup>[9a,b]</sup> Although TCBPA was superior than 4g for the azolation of PhCl, 4g was more robust for the azolation of very electron-poor dichlorobenzenes (22–38%), and even engaged highly electron-poor arenes like PhF and acetophenone (3ja and 3ka), in comparable or even higher efficiencies than previous bulkier radical cationic photocatalysts.<sup>[9a,b]</sup> For PhF, C(sp<sup>2</sup>)-F substitutive azolation was competitive with C(sp<sup>2</sup>)-H azolation – as we previously observed for acyclic TPAs<sup>[9b]</sup> – giving an impressive 59% yield of combined PhF-activated products. Overall, compared to its acyclic triarylamine predecessors that required electronic tuning to azolate (moderately) electron-rich, electron-neutral and very electron-poor arenes, DCAcridone (4g) appeared at the outset (*vide infra*) to represent a versatile, single, low M.W. ‘super’-oxidation photocatalyst precursor for a range of arenes with different electronics.

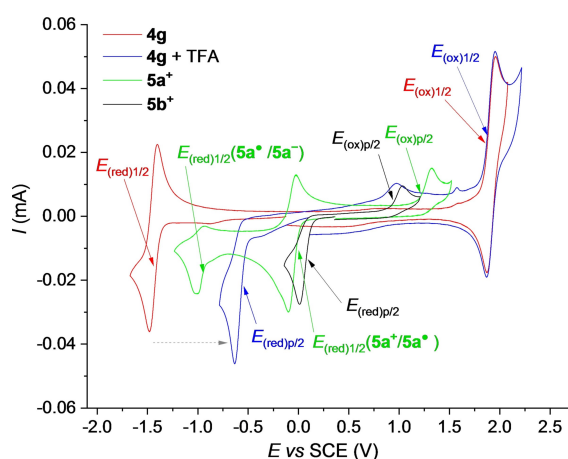


**Scheme 2.** e-PRC C–H azolation of arenes using 4g. Unless otherwise specified, isolated yields correspond to the major isomer and 1.0 mL of 1 used (≈55 equiv. 1b). [a] Yields in parenthesis of all combined isomers determined by <sup>1</sup>H NMR using 1,3,5-trimethoxybenzene as an internal standard, [b] U<sub>cell</sub> = +1.4 V was used. [c] Average of 2 replicates. [d] Inseparable mix of distinguishable products. In some cases, conversion of azole 2 was not full after 2 F mol<sup>-1</sup>.



**Mechanism:** The catalyst structure activity relationship, optimization studies and arene scope of acridone-type catalysts (**4c/4g**) revealed their key behavioral differences to phenoxazine (**4a**) and phenothiazine (**4b**) cousins. A different mechanism must operate under the photoelectrochemical reaction conditions, which we sought to understand. The cyclic voltammetry of **4g** revealed a fully-reversible SET oxidation ( $E_{1/2}(\mathbf{4g}^{\bullet+}/\mathbf{4g}) = +1.91$  V vs SCE, Figure 2). As expected, N radical cation formation is endergonic compared to phenothiazine/phenoxazine **4a/4b** (see SI, section 8.1) and also compared to acyclic TPAs due to the electron-withdrawing bridging C=O group. For acyclic TPAs, the trend between  $U_{\text{cell}}$  and product yield after a given time corresponded well with the cyclic voltammogram<sup>[9b]</sup> but this was not the case for **4g**; with notable product formation occurring prior to the onset potential in the CV (see SI, section 8.2). Thus, we initially postulated that photoexcited  $\mathbf{4g}^*$  might directly serve as the photooxidant in its neutral form rather than its radical cationic form. Although it exhibited a fully reversible wave for reduction ( $E_{1/2}(\mathbf{4g}/\mathbf{4g}^{\bullet-}) = -1.44$  V vs SCE), which in combination with the  $E_{0,0}$  energy (see SI for details) would result in an approximate excited state potential of only ( $E_{1/2}(\mathbf{4g}^{\bullet+}/\mathbf{4g}^{\bullet-}) + 1.69$  V vs SCE; this is still too low to oxidize unactivated arenes like PhCl. Indeed, Stern–Volmer quenching experiments revealed no quenching of the steady-state emission of  $\mathbf{4g}^*$  or its lifetime ( $\tau = 4.9$  ns) even up to 10000 equiv. of PhCl, although  $\mathbf{4g}^*$  was poorly emissive in the first place (see SI, section 10).

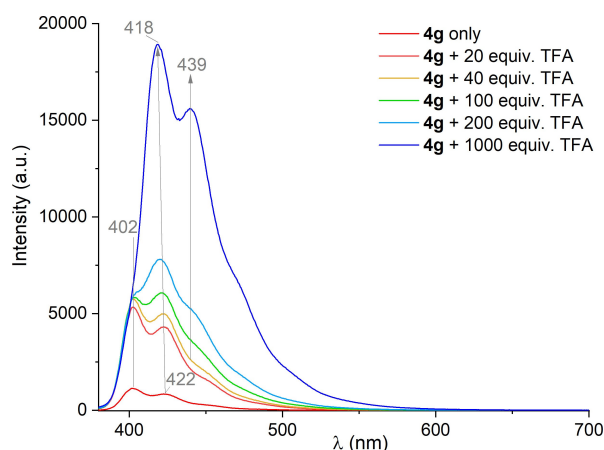
Interestingly, in the presence of TFA (200 equiv. vs **4g**) the reduction process became *substantially* (820 mV) more accessible ( $E_{\text{red}}^p = -0.64$  V vs SCE), allowing to estimate an excited state potential of ca. +2.49 V vs SCE which rivals the oxidation potential of benzene/1,2-dichlorobenzene ( $E_{\text{ox}}^p \approx 2.50$ – $2.70$  V vs SCE).<sup>[2b]</sup> The effect of TFA on the photo-physical properties of **4g** could also be observed in i) the UV/Vis by development of a shoulder at  $\approx 420$  nm (see SI, section 6.2), and ii) more obviously in the emission spectrum



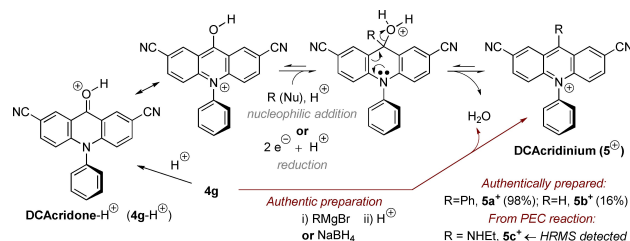
**Figure 2.** Cyclic voltammograms of **4g**, **4g** + TFA (200 equiv.), **5a<sup>+</sup>** and **5b<sup>+</sup>** (*vide infra*) 1.0 mM in MeCN (0.1 M  $t\text{Bu}_4\text{N}^+\text{PF}_6^-$ ) vs  $\text{Fc}^0/\text{Fc}^+$ . Note: Peak currents are not comparable between **4** and **5**, vs  $\text{Fc}^0/\text{Fc}^+$ ; they are all 1 electron processes.

(Figure 3), where a new peak appeared at  $\lambda_{\text{max}} = 439$  nm, as well as a notable intensity increase of the peak at  $\lambda_{\text{max}} = 422$  nm. A deshielding of aromatic protons neighboring the carbonyl group occurred in the  $^1\text{H}$  NMR (see SI, section 7). A key observation was that addition of TFA also made the SET reduction process irreversible (Figure 2, red vs blue trace). At this juncture, we hypothesized that protonated, photoexcited  $\mathbf{4g}\text{-H}^*$  was undergoing nucleophilic/reductive electron transfer decomposition. Acid promoted liberation of  $\text{H}_2\text{O}$  to afford the corresponding 2,7-dicyanoacridinium ( $\mathbf{5}^+$ ) salt would be a likely culprit (Scheme 3).<sup>[25]</sup>

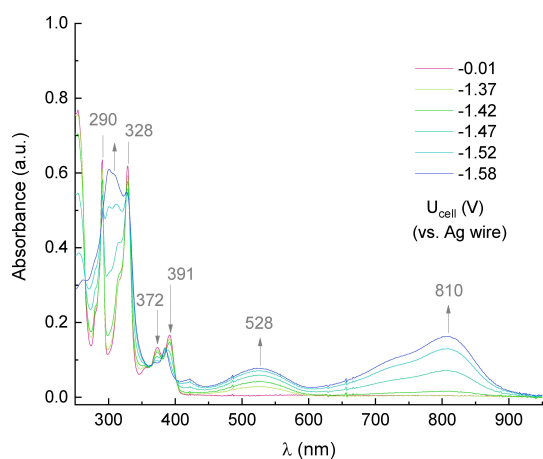
We turned to spectroelectrochemistry to observe changes in the UV/Vis absorption of reductively-activated **4g** (Figure 4). In the absence of TFA, when a cell potential ( $U_{\text{cell}} = -1.58$  V) reaching the redox potential for reduction of **4g** ( $E_{1/2} = -1.44$  V vs SCE) was applied, new peaks at  $\lambda_{\text{max}} = 428$ , 528 and 810 nm developed, the latter as a broad, charge transfer band. Upon the reverse scan ( $U_{\text{cell}} = -1.03$  V), we observed a decrease of the 810 nm peak intensity and increase of the peak intensity at 528 nm. While the nature of the former species is yet unclear,<sup>[26]</sup> we attribute the latter band ( $\lambda_{\text{max}} = 528$  nm) to the radical anion ( $\mathbf{4g}^{\bullet-}$ ). A similar broad absorption between 450–600 nm was observed for the structurally similar benzophenone radical anion.<sup>[27]</sup> In any case, signals corresponding to acridinium salt  $\mathbf{5}^+$  were not detected due to the stability of  $\mathbf{4g}^{\bullet-}$  (CV reversibility) in the absence of TFA. Unfortunately, with



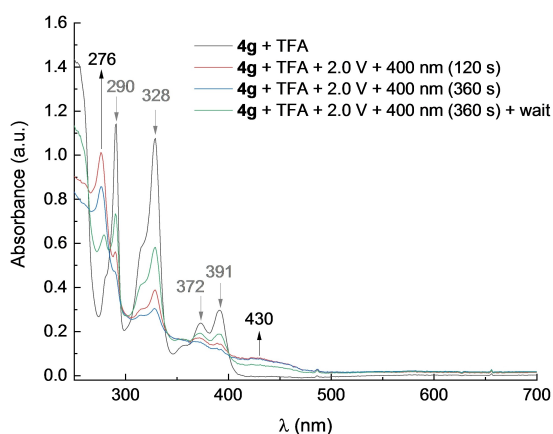
**Figure 3.** Emission ( $\lambda_{\text{ex}} = 360$  nm) of **4g** (0.05 mM) alone and in the presence of increasing concentrations of TFA in MeCN.



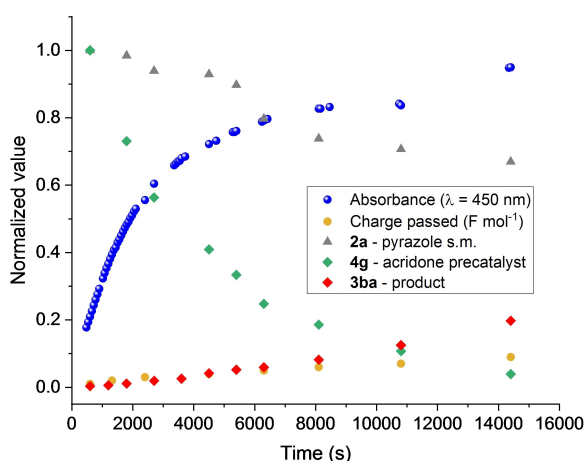
**Scheme 3.** Hypothesized acid-promoted nucleophilic/reductive decomposition of **4g** to an acridinium ( $\mathbf{5}^+$ ) salt and authentic preparations of related acridinium salts.



**Figure 4.** Spectroelectrochemistry of **4g** (1.0 mM) in MeCN (0.1 M  $t\text{Bu}_4\text{N}^+\text{PF}_6^-$ ) with increasing cathodic applied potential.



**Figure 5.** UV/Vis spectra of **4g** (1.0 mM) + TFA (100 equiv.) upon subjecting to applied anodic potential and 400 nm irradiation.



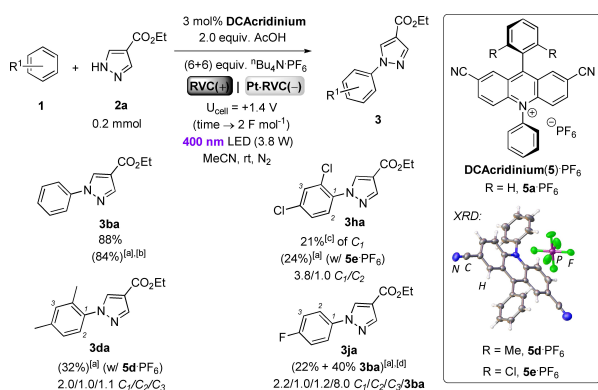
**Figure 6.** Kinetic profile for the reaction forming **3ba** at  $U_{\text{cell}} = +1.4$  V (top left), monitoring at  $\lambda_{\text{abs}} = 450$  nm. HPLC abundances of the components and absorption intensity are normalized. Charge passed ( $\text{F mol}^{-1}$ ) is absolute.

TFA present, cathodic SEC experiments were occluded by formation of bubbles on the working electrode in the thin-film UV/Vis cell (notable HER). Instead, anodic potential and 400 nm light (as per the synthetic reaction) were simultaneously applied to the spectroelectrochemical cell (Figure 5). Gratifyingly, we observed peaks corresponding to an acridinium species ( $\lambda_{\text{max}} = 276$  nm;  $\approx 420\text{--}480$  nm (broad peak), corroborating that **4g** can transform to **5<sup>+</sup>** under conditions representative of the synthetic reaction (light may not be needed for this, see SI, section 12).

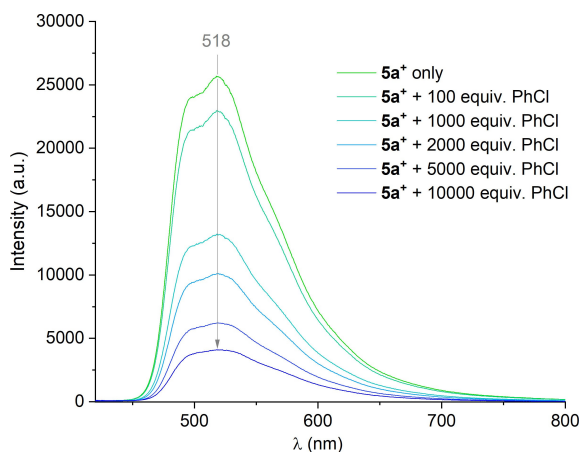
A kinetic analysis of the reaction forming **3ba** revealed how rapid consumption of **4g** in the initial hours of the reaction trended with the development of the 450 nm absorber (Figure 6). After this point, the charge passed became linear/stable and product formation increased with positive curvature, confirming that **5<sup>+</sup>** is the active e-PRC catalyst responsible for catalytic turnover. Moreover, in the absence of potential and in the presence of **1b** and TFA, irradiating **4g** led to a new peak in the LC-MS consistent with an acridinium salt species (see SI, section 11.2). To investigate further, we synthesized 2,7-dicyano-1,9-diphenylacridinium (**5a<sup>+</sup>**) and 2,7-dicyano-1-phenyl-9H-acridinium (**5b<sup>+</sup>**) hexafluorophosphate salts as surrogate authentic standards, by addition of  $\text{PhMgCl}$  to **4g** followed by acid-catalyzed elimination<sup>[25]</sup> and salt metathesis (98 % yield, see SI, section 2).<sup>[28]</sup>

Supporting the transformation of **4g** into an acridinium (**5<sup>+</sup>**) salt, the e-PRC azolation reaction using authentically synthesized **5a<sup>+</sup>** ( $\text{PF}_6^-$  salt) gave **3ba** in 88 % isolated yield. Elsewhere, there is precedent for commercial acridinium (**Mes-Acr<sup>+</sup>**) salt photocatalysts being stable under ‘recycling’ e-PRC conditions,<sup>[9c,d]</sup> albeit only allowing azolation of electron-rich arenes (e.g. anisole, mesitylene).<sup>[9d]</sup> Here, **5a<sup>+</sup>** was able to engage benzene (88 % yield of **3ba**) and 1,3-dichlorobenzene as electron-neutral and electron-deficient arenes. Since the role of TFA was primarily to assist transformation of acridone **4g** into acridinium salt **5<sup>+</sup>** as the active photocatalyst, a less strongly acidic protic source (AcOH) could be employed for the counter HER reaction, affording **3ba** in 84 % yield and **3ha** in 21 % yield (Scheme 4).

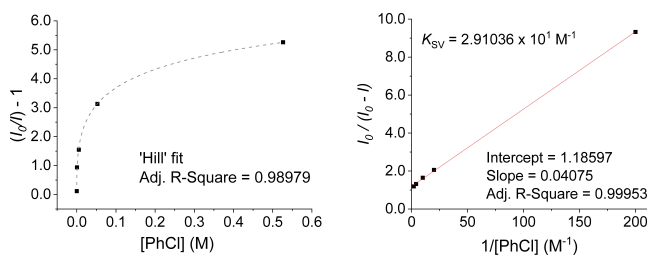
The salts **5a<sup>+</sup>**/**5b<sup>+</sup>** were even more prone to reduction than protonated **4g-H<sup>+</sup>** (by 580 mV, Figure 2) but this time in a fully reversible process ( $E_{1/2}(\text{5a}^+/\text{5a}^*) = -0.06$  V vs SCE). Based on the UV/Vis and emission spectra (see SI, section 10) this allowed to estimate an excited state potential of ( $E_{1/2}(*\text{5a}^+/\text{5a}^*) = +2.56\text{--}3.05$  V vs SCE;<sup>[29]</sup> a record<sup>[1d,7i]</sup> for acridinium salt photoredox catalysts (vs 9-mesityl-1-methylacridinium, ‘**Mes-Acr<sup>+</sup>**’:  $E_{1/2}(*\text{Mes-Acr}^+/\text{Mes-Acr}^*) = +2.06$  V vs SCE), that certainly lies within range of electron-poor arenes (benzene, dichlorobenzene). Indeed, strong luminescence quenching of **5a<sup>+</sup>** (Figure 7) by PhCl was observed. The resulting Stern–Volmer plot was non-linear and displayed strong negative deviation, revealing that a fraction of the quencher population was inaccessible. Fitting with the Lehrer equation<sup>[30]</sup> yielded a linear plot and provided a high quenching rate constant of  $k_q = 8.90 \times 10^9 \text{ M}^{-1} \text{ s}^{-1}$  (Figure 8). This is at the diffusion limit in MeCN ( $10^{10} \text{ M}^{-1} \text{ s}^{-1}$ )<sup>[1d,31]</sup> and can only be explained by a



**Scheme 4.** e-PRC C–H azolation of arenes **1** (1.0 mL,  $\approx 55$  equiv. **1b**) using **5<sup>+</sup>**. Isolated yields not in parenthesis. [a] Yield in parenthesis (combined for all combined isomers where appropriate) determined by  $^1\text{H}$  NMR using 1,3,5-trimethoxybenzene as an internal standard, [b] TFA instead of AcOH, [c] 10 equiv. of AcOH were used. [d] inseparable mixture of distinguishable products.

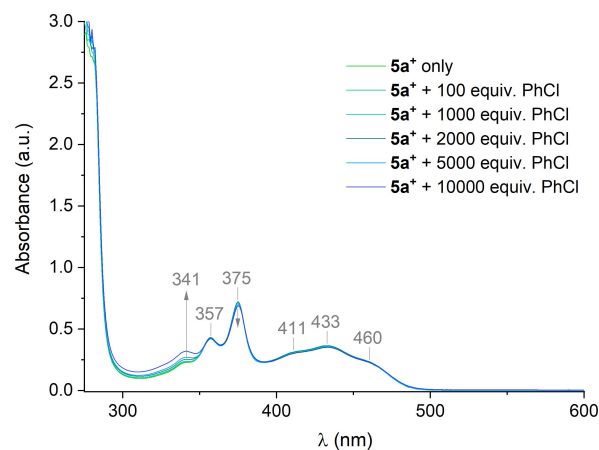


**Figure 7.** Quenching of the emission of **5a<sup>+</sup>** (0.05 mM) by [PhCl] in MeCN.



**Figure 8.** Stern–Volmer (left) vs Lehrer (right) equation fitting.

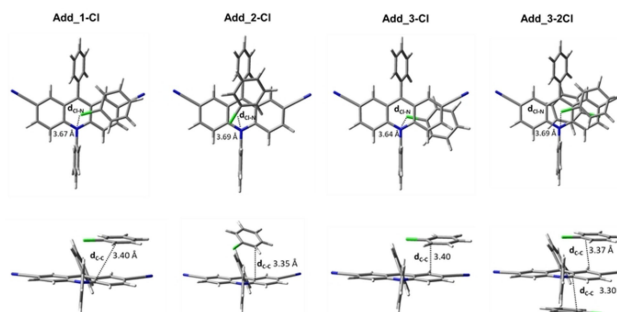
preassembly of PhCl molecules with **5a<sup>+</sup>** prior to photoexcitation. Lehrer fitting for quenching of **5a<sup>+</sup>** by PhH (see SI, section 10) also provided a high quenching rate constant of  $k_q = 3.67 \times 10^9 \text{ M}^{-1} \text{ s}^{-1}$ . At increasing [PhCl], a minor growth of the shoulder at  $\lambda_{\text{max}} = 341 \text{ nm}$  developed in the UV/Vis spectrum (Figure 9), but not so for PhH (see SI, section 6.2).



**Figure 9.** Influence of [PhCl] on the absorption of **5a<sup>+</sup>** (0.05 mM) in MeCN.

This is an indication for a preassembly of **5a<sup>+</sup>** with PhCl at high [PhCl], mirroring our previous observation that the UV/Vis spectrum of **TPA<sup>+</sup>**s changes in the presence of unsymmetrical arenes (PhCl) but not in the presence of symmetrical arenes (mesitylene).<sup>[9b]</sup> Clearly, detection of photocatalyst-substrate preassembly by steady-state methods requires a substrate with a strong dipole (or quadrupole) in order to provide a sufficient shift in charge density at the chromophore. The lifetime of **5a<sup>+</sup>** measured by TCSPC was 3.6 ns. Thus, although **5a<sup>+</sup>** lives long enough for diffusion-controlled photochemistry, its reaction with arenes nonetheless occurs via static quenching in a preassembly of PhCl molecules. The preassembly of **5a<sup>+</sup>** with one and two PhCl molecules was further investigated by density functional theory (DFT) calculations. Three initial candidate geometries were considered, and the corresponding final structures all converged to afford  $\pi$ - $\pi$  stacked assemblies in which the Cl atom pointed towards the cationic N atom of the acridinium core (Figure 10).

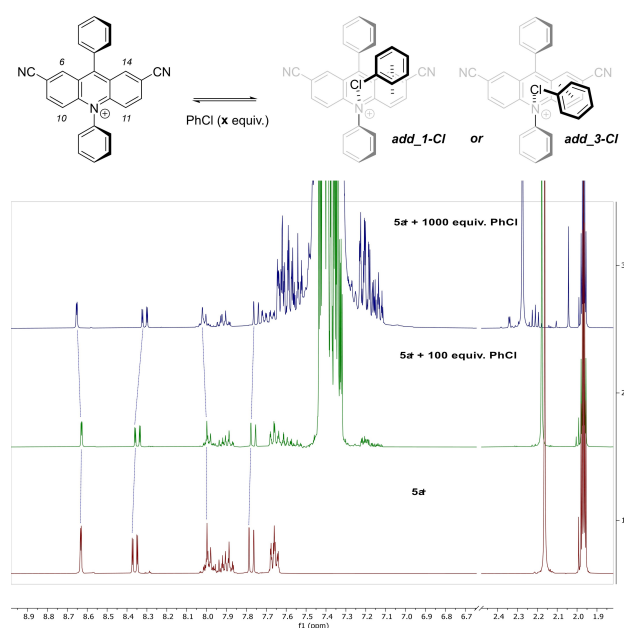
The through-space electrostatic Cl...N interaction<sup>[32]</sup> acts as driving force for stabilizing the assemblies, favoring the  $\pi$ - $\pi$  stacking assembly over any T- $\pi$  assemblies at the N- or 9-aryl substituents. For symmetrical arene PhH, formation of assemblies was more endergonic (see SI, section 15). In the



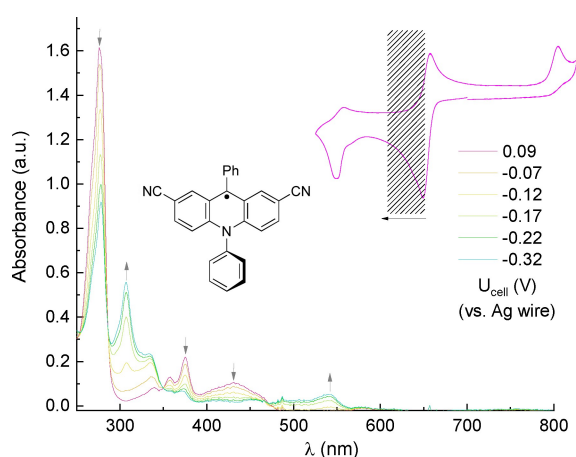
**Figure 10.** Top view (top row) and side view (bottom row) of the preassemblies of **5a<sup>+</sup>** with one (add\_1-Cl / add\_2-Cl / add\_3-Cl) and two (add\_3-2Cl) PhCl molecules.



absence of a strong dipole in PhH, a T- $\pi$  assembly at the *N*-aryl substituent also converged. However, for both PhCl and PhH, the  $\pi$ - $\pi$  stacking interaction consistently led to more stable adducts with respect to the T- $\pi$  modes. Treating **5a**<sup>+</sup> at the synthetic reaction concentration with increasing [PhCl] (up to 1000 equiv.; representing 10 equiv. w.r.t. azole in the synthetic reaction) in MeCN-d<sub>3</sub> led in the <sup>1</sup>H NMR to deshielding of **5a**<sup>+</sup>'s aromatic protons at the 6-/14- positions, while protons at the 10-/11- positions became shielded (Figure 11). This consists with a  $\pi$ - $\pi$  stacked assembly in which the Cl atom in close proximity to the cationic N atom provides shielding electron density that decreases the inductive effect of the cationic N atom.



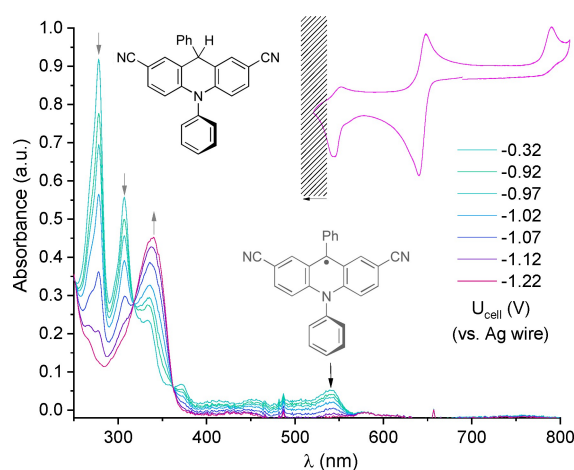
**Figure 11.** NMR study of preassembly of **5a**<sup>+</sup> (5.0 mM) with PhCl in MeCN-d<sub>3</sub>.



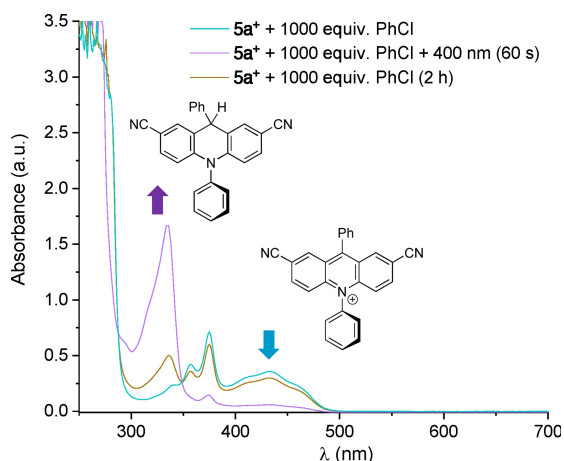
**Figure 12.** Spectroelectrochemistry of **5a**<sup>+</sup> (1.0 mM) in MeCN (0.1 M) with increasing cathodic applied potential with an overlay of the cyclic voltammogram (Figure 2), matching potential ranges of first reduction event: stepwise formation of acridine radical.

Now knowing that a 2,7-dicyanated acridinium salt **5**<sup>+</sup> (not an acridone) was the active catalyst, we sought to confirm a 'recycling' e-PRC mechanism whereby the role of electrochemistry is to regenerate **5a**<sup>+</sup> as the photocatalyst. SEC analysis of **5a**<sup>+</sup> in MeCN revealed formation of the acridine radical **5a**<sup>•</sup> when applied potentials ( $U_{\text{cell}} = -0.1 \rightarrow -0.3$  V; Figure 12) reached the redox potential of the first, fully-reversible SET reduction event (Figure 2, green trace,  $E_{1/2} = -0.06$  V vs SCE), and the observed spectra was fully consistent with the literature for a related acridine radical.<sup>[6d]</sup> At higher applied potentials ( $U_{\text{cell}} = -0.9 \rightarrow -1.2$  V) reaching the second, quasi-reversible reduction event ( $E_{1/2} = -0.99$  V vs SCE), **5a**<sup>•</sup> was further reduced, arising a species with  $\lambda_{\text{max}} = 340$  nm (Figure 13). This species was assigned as **5a-H**, presumably by protonation of acridinide anion **5a**<sup>-</sup>, since addition of NaBH<sub>4</sub> to **5a**<sup>+</sup> gave exactly the same absorption profile. This explains the quasi-reversibility of the second SET reduction event in the CV. Electrochemical detection of acridinide anions has only been reported once, with *N*-methyl-9,10-dihydroacridine being reduced at a potential of ( $E_{\text{red}}^{\text{p}} = -1.50$  V vs SCE in DMSO).<sup>[33]</sup> Related acridinide anions (without stabilizing cyano groups) are known to only be stable enough to observe by NMR in liq. NH<sub>3</sub>.<sup>[34]</sup> To confirm which species was formed in the photochemical step of the reaction, we irradiated **5a**<sup>+</sup> with 400 nm in the presence of 1000 equiv. PhCl (Figure 14) – conditions representative of the synthetic reaction.

To our surprise, we observed exclusively **5a-H** (the same behaviour was observed for PhH, see SI, section 6.3) Therefore, the photoexcited state (**\*5a**<sup>+</sup>) undergoes *rapid two electron reduction*.<sup>[35–37]</sup> Such reactivity of photoexcited acridinium salts is novel, and contrasts with the acridine radicals derived from less electron-poor acridinium salts that have been demonstrated as potent photoreductants.<sup>[6d]</sup> A two-electron oxidation of a single arene molecule to its dication would be highly unfavorable, therefore we propose that *two PhCl molecules are oxidized in concert* by **\*5a**<sup>+</sup> via SET. This is supported by i) the observation of a



**Figure 13.** Spectroelectrochemistry of **5a**<sup>+</sup> (1.0 mM) matching second reduction event: reduction of acridine radical to acridinide anion, rapid protonation to **5a-H**.

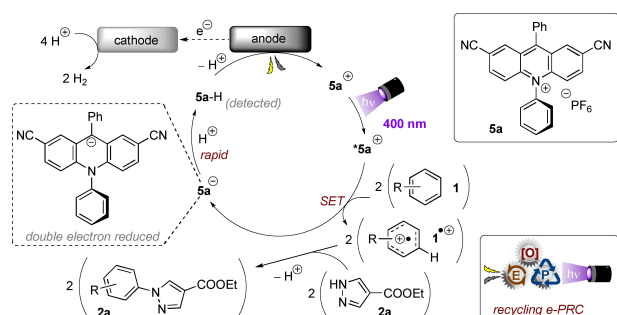


**Figure 14.** UV/Vis spectra upon irradiation of  $5a^+$  (0.05 mM) in presence of PhCl.

preassembly of  $5a^+$  and PhCl in the steady state UV/Vis spectrum (Figure 9) and ii) a quenching rate constant ( $\approx 10^{10}$ ) at the diffusional limit. The resulting arene radical cations go on to react in azolations and thereafter our proposed mechanism for the arene azolation is based on the ‘recycling’ e-PRC mechanism of Xu and co-workers<sup>[9d]</sup> with **Mes-Acr**<sup>+</sup> (Scheme 5). The acridinide anion is rapidly protonated and then reoxidized to  $5a^+$  at the anode while liberating a proton. Alternatively, the acridinide anion is reoxidized to the acridine radical (either anodically or by reduction of protons to  $H_2$ ) which reduces the intermediate following addition of pyrazole to the arene radical cation.

## Conclusion

Herein, we report electron-deficient 2,7-dicyanated acridones and acridinium salts as potent, closed-shell photooxidants that undergo surprising mechanisms. When acyclic triarylamine catalysts are bridged with a carbonyl group (acridones), this completely diverts their behavior away from open-shell, radical cationic, photocatalysis to closed-shell, neutral photocatalysis. Brønsted acid activation of acridones dramatically increases their susceptibility to reduction ( $\Delta E_{1/2} \approx 0.8$  V). SET reduced protonated acridones



**Scheme 5.** Proposed mechanism for recycling e-PRC.

liberate water to furnish electron-deficient acridinium salts which are very powerful photooxidants (as high as  $*E_{1/2} = +2.56$ – $3.05$  V vs SCE). As the most oxidizing acridinium salt photocatalysts disclosed to date, their excited states can oxidize even electron-deficient arenes where conventional acridinium salt photooxidants are limited only to electron-rich arenes and styrenes. Surprisingly, our 2,7-dicyanated acridinium salts appear to function via a novel mechanism that is different to conventional acridinium salts – upon photoexcitation they undergo *two electron reductive quenching* to form acridinide species, whose protonated forms were spectroscopically detected. This unique behaviour – enabled by a preassembly of ground state acridinium salt and multiple arene substrates – offers the potential to uncover new photochemical mechanisms and increase catalytic turnover in acridinium salt photoredox catalysis.

In summary, our study reveals the importance of two phenomena that are typically overlooked in photoredox catalysis: (i) catalyst decomposition/transformation under the reaction conditions to a more active catalyst and (ii) how photocatalyst-substrate preassemblies govern excited state mechanisms not only for open-shell (ps-lived) excited states<sup>[9b,14]</sup> but also for conventional, closed-shell (ns-lived) excited-state photocatalysts.

## Author Contributions

J. Ž. synthesized all catalysts, conducted the major effort on optimization of the PEC reaction conditions, synthesized and purified all azole products and wrote up experimental details in the Supporting Information file. S. B. conducted all spectroscopic mechanistic studies including NMR, UV/Vis, spectroelectrochemistry, steady state and time-resolved emission measurements. S. B. conducted the majority of LC-MS analyses and co-wrote the majority of the Supporting Information file. S. W. identified initial PEC reaction conditions and screened all catalysts. V. B. contributed all computational studies and wrote all computational parts of the manuscript and Supporting Information file. S. S. made minor contributions to reaction optimization, scope and initial catalyst screening as well as testing different 9-aryl-substituted acridiniums. J. Ž. initially prepared Pt-RVC, and S. S. optimized the platinization process (see SI for procedures). M. D. performed the kinetic study, supported J. Ž. in synthesis of catalysts and contributed to synthesis of brominated precursors. T. S. supervised and guided S. B. in mechanistic studies and provided infrastructural support to J. Ž. for initial syntheses of catalysts at IOCB Prague during a student exchange placement. J. P. B. conceptualized and led the project, wrote the manuscript, co-wrote the majority of the Supporting Information file, guided and supervised J. Ž., S. W., S. S., M. D. in their contributions, remotely guided S. B. in the late stages of experimental mechanistic studies and dealt with peer-review of the manuscript.

## Acknowledgements

J. Ž., S. W., S. S., M. D. and J.P.B. thank the Alexander von Humboldt Foundation for funding, provided within the framework of the Sofja Kovalevskaja Award endowed to J.P.B. by the German Federal Ministry of Education and Research. J. Ž. and S. S. are grateful for funding provided by the SynCat programme of the Elite Network of Bavaria and by the University of Regensburg. We thank Prof. Burkhard König for providing infrastructural support to J. Ž. at the beginning of his Master Thesis. We thank Regina Hoheisel for assistance and training in cyclic voltammetry, Dr. Marc Schlosser and Ulrike Schiessl for SEM analysis. Wolfgang Haumer for checking the analysis of lifetime measurements, and Reji-Idiculla Roshen for measuring UV/Vis samples of acridone derivatives. S. B. and T. S. thank the IOCB Prague for institutional support. V. B. thanks the IT4Innovations National Supercomputer Center, supported by The Ministry of Education, Youth and Sports from the Large Infrastructures for Research, Experimental Development CzechNanoLab Research Infrastructure supported by MEYS CR (LM2023051). J. P. B. is an associated member of DFG TRR 325 'Assembly Controlled Chemical Photocatalysis' (444632635) and thanks other members of the TRR for insightful discussions. Open Access funding enabled and organized by Projekt DEAL.

## Conflict of Interest

The authors declare no conflict of interest.

## Data Availability Statement

The data that support the findings of this study are available in the supplementary material of this article.

**Keywords:** Acridinium • Acridone • Photoelectrochemistry • Photoredox Catalysis • Preassembly

- [1] For selected reviews, see: a) J. M. R. Narayanam, C. R. J. Stephenson, *Chem. Soc. Rev.* **2011**, *40*, 102–113; b) C. Prier, D. Rankic, D. W. C. MacMillan, *Chem. Rev.* **2013**, *113*, 5322–5363; c) S. Fukuzumi, K. Ohkubo, *Chem. Sci.* **2013**, *4*, 561–574; d) N. A. Romero, D. A. Nicewicz, *Chem. Rev.* **2016**, *116*, 10075–10166; e) K. L. Skubi, T. R. Blum, T. P. Yoon, *Chem. Rev.* **2016**, *116*, 10035–10074; f) J. K. Matsui, S. B. Lang, D. R. Heitz, G. A. Molander, *ACS Catal.* **2017**, *7*, 2563–2575.
- [2] For selected reviews dedicated to the field of e-PRC: a) J. P. Barham, B. König, *Angew. Chem. Int. Ed.* **2020**, *59*, 11732–11747; *Angew. Chem.* **2020**, *132*, 11828–11844; b) S. Wu, J. Kaur, T. A. Karl, X. Tian, J. P. Barham, *Angew. Chem. Int. Ed.* **2022**, *61*, e202107811; *Angew. Chem.* **2022**, *134*, e202107811; c) H. Huang, K. A. Steiniger, T. H. Lambert, *J. Am. Chem. Soc.* **2022**, *144*, 12567–12583; d) A. Jorea, L. Dell'Amico, G. Goti, D. Ravelli, *Photochemistry electrified: pushing the boundaries of radical-based organic synthesis in Photochemistry: Vol. 50* (Eds: S. Crespi, S. Protti), Royal Society of Chemistry, London, **2023**, Ch. 11.
- [3] For selected reviews partially covering the field of e-PRC: a) T. H. Meyer, I. Choi, C. Tian, L. Ackermann, *Chem* **2020**, *6*, 2484–2496; b) L. F. T. Novaes, J. Liu, Y. Shen, L. Lu, J. M. Meinhardt, S. Lin, *Chem. Rev.* **2021**, *50*, 7941–8002; c) S. H. Park, M. Ju, A. J. Ressler, J. Shim, H. Kim, S. Lin, *Aldrichimica Acta* **2021**, *54*, 17–27.
- [4] For selected reviews partially covering the field of conPET: a) F. Glaser, C. Kerzig, O. S. Wenger, *Angew. Chem. Int. Ed.* **2020**, *59*, 10266–10284; *Angew. Chem.* **2020**, *132*, 10350–10370; b) J. Castellanos-Soriano, J. C. Herrera-Luna, D. D. Díaz, M. Consuelo Jiménez, R. Pérez-Ruiz, *Org. Chem. Front.* **2020**, *7*, 1709–1716; c) S. Reischauer, B. Pieber, *iScience* **2021**, *24*, 102209; d) D. De Vos, Karthik Gadde, B. U. W. Maes, *Synthesis* **2023**, *55*, 193–231.
- [5] Selected examples of potent reducing closed-shell photocatalysts ( $E_{1/2} \geq -2.0$  V vs SCE): a) Y. Du, R. M. Pearson, C.-H. Lim, S. M. Sartor, M. D. Ryan, H. Yang, N. H. Damrauer, G. M. Miyake, *Chem. Eur. J.* **2017**, *23*, 10962–10968; b) J. I. Bardagi, I. Ghosh, M. Schmalzbauer, T. Ghosh, B. König, *Eur. J. Org. Chem.* **2018**, 34–40; c) B. G. McCarthy, R. M. Pearson, C.-H. Lim, S. M. Sartor, N. H. Damrauer, G. M. Miyake, *J. Am. Chem. Soc.* **2018**, *140*, 5088–5101; d) E. Speckmeier, T. G. Fischer, K. Zeitler, *J. Am. Chem. Soc.* **2018**, *140*, 15353–15365; e) C. Kerzig, O. S. Wenger, *Chem. Sci.* **2019**, *10*, 11023–11029; f) S. Jin, H. T. Dang, G. C. Haug, R. He, V. D. Nguyen, V. T. Nguyen, H. D. Arman, K. S. Schanze, O. V. Larionov, *J. Am. Chem. Soc.* **2020**, *142*, 1603–1613; g) During the review of this manuscript, a potent and general catalyst for deep reductions was reported, see: S. Wu, F. Schiel, P. Melchiorre, *Angew. Chem. Int. Ed.* **2023**, *62*, e202306364; *Angew. Chem.* **2023**, *135*, e202306364.
- [6] Selected examples of single catalytic systems for reductive conPET: a) I. Ghosh, T. Ghosh, J. I. Bardagi, B. König, *Science* **2014**, *346*, 725–728; b) M. Neumeier, D. Sampedro, M. Májek, V. A. de la Peña O'Shea, A. Jacobi von Wangelin, R. Pérez-Ruiz, *Chem. Eur. J.* **2018**, *24*, 105–108; c) J. P. Cole, D.-F. Chen, M. Kudisch, R. M. Pearson, C.-H. Lim, G. M. Miyake, *J. Am. Chem. Soc.* **2020**, *142*, 13573–13581; d) I. A. MacKenzie, L. Wang, N. P. R. Onuska, O. F. Williams, K. Begam, A. M. Moran, B. D. Duneitz, D. A. Nicewicz, *Nature* **2020**, *580*, 76–80; e) S. Caby, L. M. Bouchet, J. E. Argüello, R. A. Rossi, J. I. Bardagi, *ChemCatChem* **2021**, *13*, 3001–3009; f) J. Xu, J. Cao, X. Wu, H. Wang, X. Yang, X. Tang, R. W. Toh, R. Zhou, E. K. L. Yeow, J. Wu, *J. Am. Chem. Soc.* **2021**, *143*, 13266–13273; g) A. F. Chmiel, O. P. Williams, C. P. Chernowsky, C. S. Yeung, Z. K. Wickens, *J. Am. Chem. Soc.* **2021**, *143*, 10882–10889; h) J. Soika, C. McLaughlin, T. Nevelsely, C. G. Daniliuc, J. J. Molloy, R. Gilmour, *ACS Catal.* **2022**, *12*, 10047–10056; i) 'Tandem' catalytic systems for multiple photon energy harvesting are also known, see Refs. 4a,d and: F. Glaser, O. S. Wenger, *J. Am. Chem. Soc. Au* **2022**, *2*, 1488–1503; j) M. L. Czyn, M. S. Taylor, T. H. Horngren, A. Polyzos, *ACS Catal.* **2021**, *11*, 5472–5480.
- [7] Selected examples of potent oxidizing closed-shell photocatalysts ( $E_{1/2} \geq +2.0$  V vs SCE): a) S. Fukuzumi, H. Kotani, K. Ohkubo, S. Ogo, N. V. Tkachenko, H. Lemmetyinen, *J. Am. Chem. Soc.* **2004**, *126*, 1600–1601; b) N. A. Romero, K. A. Margrey, E. N. Tay, D. A. Nicewicz, *Science* **2015**, *349*, 1326–1330; c) L. Niu, H. Yi, S. Wang, T. Liu, J. Liu, A. Lei, *Nat. Commun.* **2017**, *8*, 14226; d) R. Hauptmann, A. Petrosyan, F. Fennel, M. A. Argüello Cordero, A.-E. Surkus, J. Pospech, *Chem. Eur. J.* **2019**, *25*, 4325–4329; e) B. Zilante, C. Fischer, L. Schneider, C. Sparr, *Synthesis* **2019**, *51*, 4359–4365; f) A. Gini, T. Rigotti, R. Pérez-Ruiz, M. Uygur, R. Mas-Ballesté, I. Corral, L. Martínez-Fernández, V. A. de la Peña O'Shea, O. García Mancheño, J. Alemán, *ChemPhotoChem* **2019**, *3*, 609–612; g) T. Taeufer, R. Hauptmann, F. El-Hage, T. S. Mayer, H.



- Jiao, J. Rebeah, J. Pospech, *ACS Catal.* **2021**, *11*, 4862–4869; h) Q. Y. Li, L. A. Hunt, K. H. Wijesinghe, C. Curiaç, A. Williams, A. Dass, N. I. Hammer, J. H. Delcamp, *Adv. Energy Mater.* **2023**, *13*, 2203102; i) For selected reviews on acridinium and cyanoarene-type catalysts, see: B. Zilate, C. Fischer, C. Sparr, *Chem. Commun.* **2020**, *56*, 1767–1775; j) A. Tlili, S. Lakhdar, *Angew. Chem. Int. Ed.* **2021**, *60*, 19526–19549; *Angew. Chem.* **2021**, *133*, 19678–19701; k) P. Natarajan, B. König, *Eur. J. Org. Chem.* **2021**, 2145–2161.
- [8] Selected examples of oxidative conPET: a) D. Rombach, H.-A. Wagenknecht, *ChemCatChem* **2018**, *10*, 2955–2961; b) D. Rombach, H.-A. Wagenknecht, *Angew. Chem. Int. Ed.* **2020**, *59*, 300–303; *Angew. Chem.* **2020**, *132*, 306–310; c) K. Targos, O. P. Williams, Z. K. Wickens, *J. Am. Chem. Soc.* **2021**, *143*, 4125–4132.
- [9] Selected examples of oxidative e-PRC (radical cationic and closed-shell catalysts with  $*E_{1/2} \geq +2.0$  V vs SCE): a) H. Huang, Z. M. Strater, M. Rauch, J. Shee, T. J. Sisto, C. Nuckolls, T. H. Lambert, *Angew. Chem. Int. Ed.* **2019**, *58*, 13318–13322; *Angew. Chem.* **2019**, *131*, 13452–13456; b) S. Wu, J. Žurauskas, M. Domański, P. S. Hitzfeld, V. Butera, D. J. Scott, J. Rehbein, A. Kumar, E. Thyraug, J. Hauer, J. P. Barham, *Org. Chem. Front.* **2021**, *8*, 1132–1142; c) Y. Qiu, A. Scheremetjew, L. H. Finger, L. Ackermann, *Chem. Eur. J.* **2020**, *26*, 3241–3246; d) Z.-W. Hou, H.-C. Xu, *ChemElectroChem* **2021**, *8*, 1571–1573; e) H. Huang, T. H. Lambert, *Angew. Chem. Int. Ed.* **2021**, *60*, 11163–11167; *Angew. Chem.* **2021**, *133*, 11263–11267; f) T. Shen, T. H. Lambert, *Science* **2021**, *371*, 620–626.
- [10] Selected examples: a) S. Amthor, B. Noller, C. Lambert, *Chem. Phys.* **2005**, *316*, 141–152; b) J. A. Christensen, B. T. Phelan, S. Chaudhuri, A. Acharya, V. S. Batista, M. R. Wasielewski, *J. Am. Chem. Soc.* **2018**, *140*, 5290–5299; c) A. Ortiz, A. Pardo, J. I. Fernández-Alonso, *J. Pharm. Sci.* **1980**, *69*, 378–380; d) D. A. Corbin, B. G. McCarthy, Z. van de Lindt, G. M. Miyake, *Macromolecules* **2021**, *54*, 4726–4738.
- [11] J.-C. Moutet, G. Reverdy, *Tetrahedron Lett.* **1979**, *20*, 2389–2392.
- [12] Static and non-stationary quenching regimes without significant diffusion can occur for photoexcited radical anion photocatalysts if the substrate excess with respect to ground state radical anion catalyst is sufficiently enormous ( $>0.3$  M for a 60–200  $\mu\text{M}$ , thus  $>1500$ – $5000$  equiv.) and only for electron-deficient arenes with a driving force of  $>\text{ca. } 0.2$  eV, see: a) C. J. Zeman IV, S. Kim, F. Zhang, K. S. Schanze, *J. Am. Chem. Soc.* **2020**, *142*, 2204–2207; b) J. S. Beckwith, A. Aster, E. Vauthey, *Phys. Chem. Chem. Phys.* **2022**, *24*, 568–577.
- [13] a) X. Tian, T. A. Karl, S. Reiter, S. Yakubov, R. de Vivie-Riedle, B. König, J. P. Barham, *Angew. Chem. Int. Ed.* **2021**, *60*, 20817–20825; *Angew. Chem.* **2021**, *133*, 20985–20993; b) L. Wylie, J. P. Barham, B. Kirchner, *ChemPhysChem* **2023**, e202300470.
- [14] Evidence of preassemblies in radical ion photocatalysis was recently disclosed by observation of substrate quenching of picosecond-lived radical ion excited states in both reductive and oxidative directions, see: a) D. Y. Jeong, D. S. Lee, H. L. Lee, S. Nah, J. Y. Lee, E. J. Cho, Y. You, *ACS Catal.* **2022**, *12*, 6047–6059; b) A. Kumar, P. Malevich, L. Mewes, S. Wu, J. P. Barham, J. Hauer, *J. Chem. Phys.* **2023**, *158*, 144201.
- [15] a) Y. Kwon, J. Lee, Y. Noh, D. Kim, Y. Lee, C. Yu, J. C. Roldao, S. Feng, J. Gierschner, R. Wannemacher, M. S. Kwon, *Nat. Commun.* **2023**, *14*, 92; b) S. Horsewill, G. Hierlmeier, Z. Farasat, J. P. Barham, D. J. Scott, *ACS Catal.* **2023**, *13*, 9392–9403.
- [16] a) M. Marchini, A. Gualandi, L. Mangozzi, P. Franchi, M. Lucarini, P. G. Cozzi, V. Balzani, P. Ceroni, *Phys. Chem. Chem. Phys.* **2018**, *20*, 8071–8076; b) A. J. Rieth, M. I. Gonzalez, B. Kudisch, M. Nava, D. G. Nocera, *J. Am. Chem. Soc.* **2021**, *143*, 14352–14359.
- [17] a) C. Kerzig, X. Guo, O. S. Wenger, *J. Am. Chem. Soc.* **2019**, *141*, 2122–2127; b) see Ref. 6c.
- [18] Solvated electrons are also proposed to be evolved by neutral excited state radical species in photocatalytic reactions, see: R. Obertfk, J. Chudoba, J. Šturala, J. Tarábek, L. Ludvíková, T. Slanina, B. König, R. Cibulka, *Chem. Eur. J.* **2022**, *28*, e202202487.
- [19] For selected examples that elegantly showed a situation more complex than the initially-drawn mechanism, see: a) K. Goliszewska, K. Rybicka-Jasińska, J. A. Clark, V. I. Vullev, D. Gryko, *ACS Catal.* **2020**, *10*, 5920–5927; b) B. G. Stevenson, E. H. Spielvogel, E. A. Loiaconi, V. M. Wambua, R. V. Nakhmiyayev, J. R. Swierk, *J. Am. Chem. Soc.* **2021**, *143*, 8878–8885; for a critical perspective, see: c) T. Noël, E. Zysman-Colman, *Chem Catal.* **2022**, *2*, 468–476.
- [20] a) L. Zeng, T. Liu, C. He, D. Shi, F. Zhang, C. Duan, *J. Am. Chem. Soc.* **2016**, *138*, 3958–3961; b) E. Alfonso, A. B. Beeler, *Chem. Sci.* **2019**, *10*, 7746–7754; c) M. J. P. Mandigma, J. Žurauskas, C. I. MacGregor, L. J. Edwards, A. Shahin, L. d'Heureuse, P. Yip, D. J. S. Birch, T. Gruber, J. Heilmann, M. P. John, J. P. Barham, *Chem. Sci.* **2022**, *13*, 1912–1924.
- [21] M. J. P. Mandigma, J. Kaur, J. P. Barham, *ChemCatChem* **2023**, *15*, e202201542.
- [22] a) K. Donabauer, M. Maity, A. L. Berger, G. S. Huff, S. Crespi, B. König, *Chem. Sci.* **2019**, *10*, 5162–5166; b) C. P. Chernowsky, A. F. Chmiel, Z. K. Wickens, *Angew. Chem. Int. Ed.* **2021**, *60*, 21418–21425; *Angew. Chem.* **2021**, *133*, 21588–21595; c) J. C. Bawden, P. S. Francis, S. DiLuzio, D. J. Hayne, E. H. Doeven, J. Truong, R. Alexander, L. C. Henderson, D. E. Gómez, M. Massi, B. I. Armstrong, F. A. Draper, S. Bernhard, T. U. Connell, *J. Am. Chem. Soc.* **2022**, *144*, 11189–11202.
- [23] The same deep green color was observed upon electrooxidation of TPAs in our previous study, and for isolated TPA<sup>•+</sup> salts, see Ref. 9b.
- [24] For the photochemistry of different acridone derivatives (and acridine derivatives) as photoinitiators in polymerization or photocatalysis, see: a) A. Kira, M. Koizumi, *Bull. Chem. Soc. Jpn.* **1969**, *42*, 625–630; b) M. Abdallah, H. Le, A. Hijazi, M. Schmitt, B. Graff, F. Dumur, T.-T. Bui, F. Goubard, J.-P. Fouassier, J. Lalevée, *Polymer* **2018**, *159*, 47–58; c) K. Chen, Y. Cheng, Y. Chang, E. Li, Q.-L. Xu, C. Zhang, X. Wen, H. Sun, *Tetrahedron* **2018**, *74*, 483–489; d) T. Bortolato, G. Simionato, M. Vayer, C. Rosso, L. Paoloni, E. M. Benetti, A. Sartorel, D. Leboef, L. Dell'Amico, *J. Am. Chem. Soc.* **2023**, *145*, 1835–1846; e) Y. Yang, G. A. Volpato, E. Rossin, N. Peruffo, F. Tumbarello, C. Nicoletti, R. Bonetto, L. Paoloni, P. Umari, E. Colusso, L. Dell'Amico, S. Berardi, E. Collini, S. Caramori, S. Agnoli, A. Sartorel, *ChemSusChem* **2023**, *16*, e202201980.
- [25] Acid catalyzed elimination of water from a 9-substituted acridin-9-ol is known to afford acridinium salts. A photodissociation mechanism to afford hydroxide was also proposed – however only upon UV photoexcitation – see: D. Zhou, R. Khatmullin, J. Walpita, N. A. Miller, H. L. Luk, S. Vyas, C. M. Hadad, K. D. Glusac, *J. Am. Chem. Soc.* **2012**, *134*, 11301–11303.
- [26] The UV/Vis signals bear uncanny resemblance to TPA<sup>•+</sup>s in our previous study (Ref. 9b), suggesting that the corresponding half reaction in the spectroelectrochemical cell may initially generate 4g<sup>•+</sup> that is more stable than the target 4g<sup>••</sup> to adventitious air/moisture and can diffuse away from the electrode. The former is then eliminated upon applying potential for longer time periods. Alternatively, 4g<sup>••</sup> decomposes when at low steady-state concentrations to another species responsible for these bands, and at higher steady-state concentrations 4g<sup>••</sup> can be observed.

- [27] G. Nocera, A. Young, F. Palumbo, K. J. Emery, G. Coulthard, T. McGuire, T. Tuttle, J. A. Murphy, *J. Am. Chem. Soc.* **2018**, *140*, 9751–9757.
- [28] We also synthesized **5d**-PF<sub>6</sub> and **5e**-PF<sub>6</sub>, following a reviewer's suggestion that arene substrates in the azole coupling reaction may react at the 9-position of the acridone. Both **5d**-PF<sub>6</sub> and **5e**-PF<sub>6</sub> were competent catalysts in the azolations of the corresponding 1,3-disubstituted arene substrates, however; this does not necessarily rule out catalytic activity of other 9-substituted acridiniums generated from the transformation of **4g**.
- [29] The former value is calculated using the  $E^{0-0}$  energy is the intersection of the UV/Vis absorption and steady-state emission peaks (for **5b**<sup>+</sup>, 474 nm=2.61 eV). The latter value is calculated assuming the photon energy of the actual experimental wavelength (396 nm=3.13 eV); given the known ability of preassemblies to leverage higher excited states (Ref. 2b).
- [30] a) S. S. Lehrer, *Biochemistry* **1971**, *10*, 3254–3263; b) H. S. Geethanjali, D. Nagaraja, R. M. Melavanki, R. A. Kusanur, *J. Lumin.* **2015**, *167*, 216–221.
- [31] B. H. Farnum, W. M. Ward, G. J. Meyer, *Inorg. Chem.* **2013**, *52*, 840–847.
- [32] For examples of similar through-space field effects, see: a) E. J. Grubbs, R. Fitzgerald, R. E. Phillips, R. Petty, *Tetrahedron* **1971**, *27*, 935–944; b) B. R. Beno, K.-S. Yeung, M. D. Bartberger, L. D. Pennington, N. A. Meanwell, *J. Med. Chem.* **2015**, *58*, 4383–4438.
- [33] a) J.-P. Cheng, Y. Lu, *J. Phys. Org. Chem.* **1997**, *10*, 577–584; b) the value for the Fc<sup>0</sup>/Fc<sup>+</sup> couple vs. Ag/AgCl in DMSO (0.1 M <sup>n</sup>Bu<sub>4</sub>N·PF<sub>6</sub>) from Ref. 33b was used to convert the potential in Ref. 33a to that vs Ag/AgCl, then a factor of 0.045 V used to convert to vs SCE. see: T. A. Kardaş, H. A. Özbek, Y. Akgül, F. Demirhan, *Inorg. Nano-Met. Chem.* **2017**, *47*, 1475–1479.
- [34] A. G. Anastassiou, H. S. Kasmai, M. R. Saadein, *Tetrahedron Lett.* **1980**, *21*, 3743–3746.
- [35] We cannot exclude the possibility that the EWGs allow the acridine radical itself to become a potent photooxidant (i.e., a conPET mechanism). However, we deem this highly unlikely since **5a**<sup>•</sup> is not detected at all on the timescale of the experiment and the UV/Vis absorption coefficient of **5a**<sup>•</sup> at 400 nm is low (albeit non-zero). The transfer of two electrons to \***5a**<sup>+</sup> – while rapid – could not occur simultaneously and the acridine radical is likely transiently formed; to probe this, transient absorption spectroscopy and quantum yield measurements are required. Further studies are underway on the photodynamics of \***5a**<sup>+</sup>.
- [36] We cannot rule out rapid disproportionation of (2×) **5a**<sup>•</sup> to afford **5a**<sup>-</sup> and **5a**<sup>+</sup>. However, (i) the cyclic voltammogram shows redox events 1.0 V apart and (ii) **5a**<sup>•</sup> is stable during the SEC experiments.
- [37] We cannot rule out that the acridine radical **5a**<sup>•</sup> undergoes HAT with solvent/another HAT donor to form **5a**-H. However, **5a**<sup>•</sup> absorbs poorly at 400 nm and no such reactivity was observed in Ref. 6d. Moreover, steric hinderance for 9-aryl-substituted acridiniums would disfavor this.
- [38] Deposition numbers 2233703 (**4c**), 2233702 (**4g**-DCM) and 2233704 (**5a**<sup>+</sup>-PF<sub>6</sub>) contain the supplementary crystallographic data for this paper. These data are provided free of charge by the joint Cambridge Crystallographic Data Centre and Fachinformationszentrum Karlsruhe Access Structures service.

Manuscript received: May 30, 2023

Accepted manuscript online: August 16, 2023

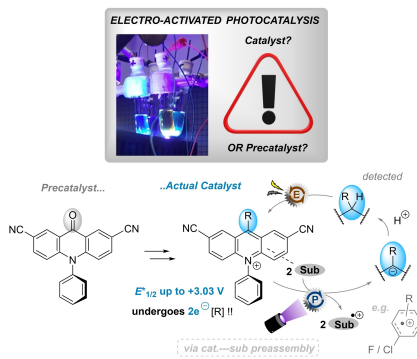
Version of record online: ■■, ■■

## Research Articles

## Photocatalysis

J. Žurauskas, S. Boháčová, S. Wu, V. Butera,  
S. Schmid, M. Domański, T. Slanina,  
J. P. Barham\* **e202307550**

Electron-Poor Acridones and Acridiniums  
as Super Photooxidants in Molecular Photo-  
electrochemistry by Unusual Mechanisms



Under photoelectrochemical conditions, dicyanated acridones are precatalysts for acridinium ions as closed-shell, highly potent arene photooxidants. Despite the lifetime permitting diffusion-controlled quenching, a preassembly with substrate nonetheless operates. Highlighting the profound influence of preassembly on photocatalysis, quenching diverts from single to double electron transfer reduction of the excited state to an acridinide anion.